Mechanics of Advanced Composite Structures 7 (2020) 89 – 101

Mechanics of Advanced Composite Structures

journal homepage: http://MACS.journals.semnan.ac.ir

Semnan University

Influence of Hygrothermal Environment and FG Material on Natural Frequency and Parametric Instability of Plates

R. Inala*

Department of Mechanical Engineering, VIT-Bhimavaram-534202, Andhra Pradesh, India

KEYWORDS

Functionally graded material plates
Temperature
Moisture
Free vibration
Dynamic stability

ABSTRACT

In this article, vibration characteristics and the parametric instability of functionally graded material (FGM) plates with cyclic loading in a hygrothermal field are discussed. The plate element is modeled in a finite element by applying the third-order shear deformation hypothesis. The mathematical formulation of the FGM plate is made with two material constituents by applying the power rule to vary in association with the thickness path of the plate. Hamilton's principle is employed to develop the arbitrary equation of motion, which is converted into periodic constants using the Mathieu Hill equation. The derived equation of movement with the help of Floquet's theorem is applied to generate the instability and stability separations of the FGM plate in the hygrothermal environment. The current proposed results are compared with existing literature results to assess its validity. The free vibration characteristics are reduced by the rise of moisture absorption and the temperature of the FGM plates in the hygrothermal atmosphere. Hence, the influence of increased parameters increases the parametric instability of FGM plates. Temperature rise and moisture absorption regarding the parametric stability and the uncertainty region of the FGM plates are also observed.

1. Introduction

The advancement of composite materials made of two or more constituent materials forms FGM. For specific applications, the FGMs are creating, which is likely possible with conventional materials. The FGMs were implemented on structural applications like automobile parts, gas turbine blades, aerospace and nuclear, etc. These structural members may be exposed to hot and moist conditions through their usage. The absorption of moisture and heat variation affects the mechanical characteristics of the FGMs. An increase in moisture concentration may generate deterioration; this affects the stiffness of plates and its dynamic stability characteristics. The FGM shell configurations can be applied to oscillatory in-plane loading. It is required to comprehend the parametric instability characteristics of the structure with different boundary conditions. This phenomenon is titled a parametric resonance of structures and has been inspected by Bolotin [1]. Parametric resonance is potentially hazardous, and the system amplitude increases exponentially even in the presence of damping. Some failures of engineering structures can be as a result of parametric resonance. Parametric uncertainty does not ensure a unique frequency value; rather, it follows over a range of frequencies. Hence, the parametric uncertainty properties of the FGM plate with hygrothermal loads are essential to study. Levinson [2] proposed a new concept for the dynamics of isotropic plates of constant thickness. The assumed displacement field allows for non-uniform shearing of a cross-section and shear-free boundary conditions. This theory provides an enhanced approximation with the concept of elasticity solution. The neutral surface concept is introduced by Zhang and Zhou [3] and applied with two constituent materials of the FGM plates. The temperature-dependent material properties proposed by Reddy and Chin [4] for thermo-mechanical properties investigate of FGM plates and cylinders. Naghdabadi and Hosseini [5] used a 3-D degenerated shell finite element applied for the thermo-elastic study of FG plates and shells. Senthil and Batra [6] deliberated the vibration analysis of supported FG shells by using a 3-D solution method.

Primarily stressed, FG plates vibration analysis in high thermal fields was reported by Yang and

* Corresponding author. Tel.: +98-863-2625720; Fax: +98-86-34173450
E-mail address: ramuinala@gmail.com

DOI: 10.22075/MACS.2019.17822.1207
Received 2019-05-13; Received in revised form 2019-08-31; Accepted 2019-10-27

Shen [7]. Their study pursuant to a change of temperature was filed by contemplating Reddy's higher-order shear deformation hypothesis. Kim [8] assumed the variation of temperature in a thickness direction of the plate for the study of rectangular FG plate vibration with high-temperature fields. Abrate [9] discussed the deflection of static plates, free vibration, and buckling of FG plates. Croce et al. [10] applied for the study of FG Reissner–Mindlin plates proposed a finite element approach. Critical buckling and natural frequency characteristics of FGM plates were computed by Ramu and Mohanty [11, 12] using the finite element method. Annular FGM plates free vibration analysis with variable thickness was established by Efraim and Eisenberger [13] applying an exact solution. Shahrjerdi et al. [14] studied the free vibration characteristics of solar FG plates in high-temperature fields by considering second-order shear deformation theory.

Researchers such as Lee studied the influence of a hygrothermal environment on stress, vibration, buckling, and dynamic stability of composite plates through various boundary conditions and Kim [15] carried out the buckling characteristics of FGM plates under hygrothermal environment. Similarly, Lee and Kim [16] examined the significance of combined thermal and moisture fields on the post-buckling performance of the FGM plate. Lal et al. [17] adopted a higher-order shear deformation hypothesis to investigate the post-buckling performance of FGM plates. Ramu and Mohanty [18] explored the effect of high thermal environments on a rotating FGM plate's dynamic instability.

Several studies have been reported the impact of hygrothermal fields on the vibration analysis of composite plates; Wanga and Dawe [19] introduced a finite strip arrangement of B-spline for the dynamic stability of prismatic plate structures and composite laminated rectangular plates. Rao and Sinha [20] inquired about the influence of moisture and temperature on the free vibration of multidirectional composites. The dynamic instability of fiber laminated composite plates subjected to a harmonic load in a heat and moisture field was analyzed by Rath and Dash [21]. Ramu [22] examined the parametric uncertainty of FG plates including parametric excitation. Ramu et al. [23] deliberated FGM effects on the vibrations due to the environment of hygrothermal. Mohammad and Hossein [24] inspected the stability analysis of higher-order refined FGM panels with aero-hygro-thermal loading. Mohammad [25] investigated the vibration analysis of layered plates by hygro-thermal loads with nonlocal stress-strain relation. FG thermal expansion coefficients are effects that thermal stability of the plate's exhibit, which was studied by Bousahla et al. [26]. Bellifa et al. [27] evaluated a four-variable discrete plate theory for the critical buckling examination of FG plates. Barati and Hossein [28] applied the nonlocal stress-strain gradient theory to study the hygro-thermal vibration analysis of graded double refined nanoplate. Youcef et al. [29] examined the trigonometric plate theory variables in order to analyse the bending analysis of S-FGM plates under hygrothermal loadings. Mohamed Zidi et al. [30] analyzed the influence of the hygro-thermo-mechanical loading on FGM plates applying a refined plate theory. Farzad and Barati [31] explore the vibration analysis of nanoscale beams with the effect of small-scale on hygro-thermo-mechanical fields. Barati [32] examined the stability analysis of porous FG nanoplates in hygro-thermal environments. Barati et al. [33] develop a higher-order refined supersonic FGM panel subjected to Aero-hygro-thermal loads to study the stability analysis. Abderrahmane et al. [34] inquired a new two-unknown trigonometric shear deformation theory to analyze the advanced nanobeams in the hygro-thermal environment. Abdelmoumen et al. [35] explored the coefficient of thermal expansion influence on the thermal stability of FG plates.

There are remarkable works associated with the vibration investigation of an FGM plate under moisture and thermal conditions. The author has focused on the importance of moisture and heat loading on natural frequencies, critical buckling, and dynamic stability of FGM plates. Plate fundamental kinematics are chosen from third-order shear deformation, and natural frequencies consequently dynamic durability study have been taken by a finite element method employing Floquet's approach. The intended performance investigated the importance of the moist and thermal field and the power rule index value approaching the free oscillation features and parametric uncertainty regions of the FGM plates. In moist and thermal fields, the rise of heat with various temperature diffusion restrictions and moisture rate affects the vibration properties as well as the dynamic stability of the FGM plates.

2. Mathematical Methodology

2.1. Formulation of the Problem

The rectangular cross-section with uniform thickness, having the length and width of the plate, has been deliberated for this analysis. Periodic loading on the rectangular FGM plate with temperature-dependent material, as described in Fig. 1.

The loading condition is as follows:

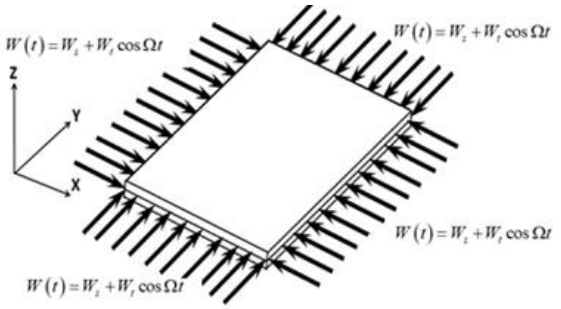

Fig.1. Biaxial periodic loading of FGM plate

$$W(t) = W_s + W_t \cos \Omega t \tag{1}$$

where *Ws* and *Wt* are static and time-dependent component of the load, correspondingly. *Ω* is the dynamic load component of the excitation frequency.

2.2. The constitutive law for FGM plate

The simple power law for varying ceramic volume portion described as below:

$$V_c(z) = \left(\frac{1}{2} + \frac{z}{h}\right)^k, 0 \le k \le \infty \tag{2}$$

where *k* index value of power law.
The effective material properties are obtained by applying the simple rule of the mixture as follows:

$$P(z) = P_c(z)V_c(z) + P_m(z)V_m(z) \tag{3}$$

where $P_c(z)$ is the ceramic material constituents and $P_m(z)$ metal material constituents about whatever location z of the neutral plane of the plate having FG material, the effective material property can be represented as P(z); it may be mass density ρ, coefficient of moisture expansion *Φ,* Poisson's ratio *v*, the elasticity of modulus *E* and thermal expansion coefficient *Ψ* of the FGM plate.
The rule of the mixture would be as follows:

$$V_C(z) + V_M(z) = 1 \tag{4}$$

2.3. Concept of the physical neutral plane

In this study, the concept of the neutral plane has been contemplated. The neutral plane concept has been adopted for this study. Fig. 2 illustrated the center plane and the neutral plane of the FGM plate.

$$d = \frac{\int_{-h/2}^{h/2} zE(z,T)dz}{\int_{-h/2}^{h/2} E(z,T)dz} \tag{5}$$

Here *d* represents the neutral and geometric middle surfaces distance.

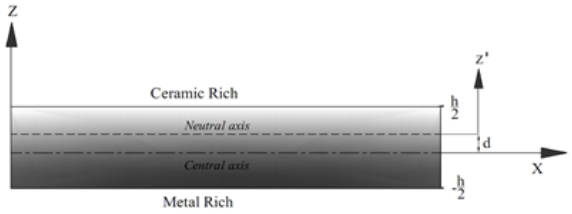

Fig. 2. The design of FG material distribution along with the thickness of the plate

2.4. The material properties are temperature-dependent

The material properties, which are temperature-dependent, acquired by the following equation:

$$P(T) = P_0\left(P_{-1}T^{-1} + 1 + P_1T + P_2T^2 + P_3T^3\right) \tag{6}$$

where P_0, P_{-1}, P_2, and P_3 are the constants of temperature and are distinctive to each constituent. $T = T_0 + T(z)$, wherever $T(z)$ is the thermal increment at any location z in accordance with depth way, and T_0 is the ambient heat.

Regarding the comparison equation (3), the active substantial features between two ingredients for FG material plates presented being developed as below:

$$\begin{aligned} E(z,T) &= E_m(T) + [E_c(T) - E_m(T)]\left(\frac{1}{2} + \frac{z}{h}\right)^k \\ \varphi(z) &= \varphi_m + [\varphi_c - \varphi_m]\left(\frac{1}{2} + \frac{z}{h}\right)^k \\ \psi(z,T) &= \psi_m(T) + [\psi_c(T) - \psi_m(T)]\left(\frac{1}{2} + \frac{z}{h}\right)^k \end{aligned} \tag{7}$$

where the subscript *m* and *c* represent metal and ceramic properties, consequently.

2.5. Fundamental kinematics

The higher progression shear deformation condition is assumed for the basic constative relation of the plate element. The normal and transverse displacement components of in-plane transposition components of the plate can be denoted as.

$$\begin{aligned} u &= u_n + z\theta_x - c_1z^3\left(\theta_x + w_{n,x}\right), \\ v &= v_n + z\theta_y - c_1z^3\left(\theta_y + w_{n,y}\right) \\ w &= w_n \end{aligned} \tag{8}$$

where u_n, v_n, w_n, θ_x and θ_y denote the purpose of x and y., u_n, v_n moreover w_n represent the displacements with respect to the inactive face of the plate. θ_x and θ_y are the circumrotation of transverse common about the y- and x- axis, accordingly.

The relationships of in-plane and transverse shear strain displacements remain expressed as below:

$$\begin{Bmatrix} \varepsilon_x \\ \varepsilon_y \\ \varepsilon_{xy} \end{Bmatrix} = \begin{Bmatrix} \varepsilon_x^{(n)} \\ \varepsilon_y^{(n)} \\ \varepsilon_{xy}^{(n)} \end{Bmatrix} + z \begin{Bmatrix} \varepsilon_x^{(1)} \\ \varepsilon_y^{(1)} \\ \varepsilon_{xy}^{(1)} \end{Bmatrix} - z^3 \begin{Bmatrix} \varepsilon_x^{(3)} \\ \varepsilon_y^{(3)} \\ \varepsilon_{xy}^{(3)} \end{Bmatrix} \tag{9}$$

$$\begin{Bmatrix} \gamma_{yz} \\ \gamma_{xz} \end{Bmatrix} = \begin{Bmatrix} \gamma_{yz}^{(n)} \\ \gamma_{xz}^{(n)} \end{Bmatrix} + z^2 \begin{Bmatrix} \gamma_{yz}^{(3)} \\ \gamma_{xz}^{(3)} \end{Bmatrix} \tag{10}$$

The stress resultants are expressed as follows:

$$\left.\begin{aligned} \begin{bmatrix} Q_{xx} \\ Q_{yy} \\ Q_{xy} \end{bmatrix} &= \int_{-h/2}^{h/2} \begin{bmatrix} \sigma_X \\ \sigma_Y \\ \tau_{XY} \end{bmatrix} dz \\ \begin{bmatrix} M_{xx} \\ M_{yy} \\ M_{xy} \end{bmatrix} &= \int_{-h/2}^{h/2} \begin{bmatrix} \sigma_X \\ \sigma_Y \\ \tau_{XY} \end{bmatrix} z dz \\ \begin{bmatrix} N_{xx} \\ N_{yy} \\ N_{xy} \end{bmatrix} &= \int_{-h/2}^{h/2} \begin{bmatrix} \sigma_X \\ \sigma_Y \\ \tau_{XY} \end{bmatrix} z^3 dz \end{aligned}\right\} \tag{11}$$

$$\left.\begin{aligned} \begin{bmatrix} S_{xz} \\ S_{yz} \end{bmatrix} &= \int_{-h/2}^{h/2} \begin{bmatrix} \tau_{XZ} \\ \tau_{YZ} \end{bmatrix} dz \\ \begin{bmatrix} R_{xz} \\ R_{yz} \end{bmatrix} &= \int_{-h/2}^{h/2} \begin{bmatrix} \tau_{XZ} \\ \tau_{YZ} \end{bmatrix} z^2 dz \end{aligned}\right\} \tag{12}$$

Substitution of eq. (10) in eq. (11) and eq. (12) yields the following relations:

$$\left.\begin{aligned} \begin{bmatrix} Q \\ M \\ N \end{bmatrix} &= \begin{bmatrix} [G] & [L] & [E] \\ [L] & [V] & [L] \\ [E] & [L] & [J] \end{bmatrix} \begin{Bmatrix} \varepsilon^{(n)} \\ \varepsilon^{(1)} \\ \varepsilon^{(3)} \end{Bmatrix} \\ \begin{bmatrix} S^s \\ R^s \end{bmatrix} &= \begin{bmatrix} [A^s] & [D^s] \\ [D^s] & [F^s] \end{bmatrix} \begin{Bmatrix} \gamma^{(n)} \\ \gamma^{(2)} \end{Bmatrix} \end{aligned}\right\} \tag{13}$$

Stiffness components are all represented as below:

$$\begin{aligned} &\left(G_{lm} \quad L_{lm} \quad V_{lm} \quad E_{lm} \quad L_{lm} \quad J_{lm}\right) \\ &= \int_{-h/2}^{h/2} Q_{lm}^{(k)} \left(1, z, z^2, z^3, z^4, z^6\right) dz \\ &(l, m = 1, 2, 6) \end{aligned} \tag{14}$$

$$\begin{aligned} &\left(A_{lm}^s \quad D_{lm}^s \quad F_{lm}^s\right) \\ &= \int_{-h/2}^{h/2} Q_{lm}^{(k)} \left(1, z^2, z^4\right) dz \\ &(l, m = 4, 5) \end{aligned} \tag{15}$$

2.6. Thermal analysis

The thickness direction is assumed to vary temperature distribution for this analysis. Uniform, linear, and nonlinear thermal environment circumstances are deliberated for this study.

2.7. Distribution of temperature uniformly

The temperature rise in accordance with thickness in the uniform temperature environment is assumed as follows:

$$T(z) = T_0 + \Delta T(z) \tag{16}$$

wherever *ΔT(z) =Tc-Tm*, represents the grade of temperature. T_c is the heat at the ceramic plane, and T_m is the temperature at the metal plane, correspondingly.

- *Analysis of temperature linearly*

The linear rise of heat on the depth is represented below as below:

$$T(z) = T_m + \Delta T(z)\left(\frac{z}{h} + \frac{1}{2}\right) \tag{17}$$

- *Distribution of temperature nonlinearly*

The nonlinear heat rise along the depth direction can be denoted as follows:

$$T(z) = T_m + (T_c - T_m) \frac{\int_{-h/2}^{z} \frac{1}{K(z)} dz}{\int_{-h/2}^{h/2} \frac{1}{K(z)} dz} \tag{18}$$

2.8. Finite Element Analysis

FGM plate model analysis has been performed by finite element procedure applying a rectangular element with four-node as depicted in Fig.3. Each node contains seven degrees of freedom. The normal displacements fields are *u, v* and *w* is the oblique displacement, θ_x and θ_y circumrotation with respective x and y-axis, correspondingly. Similarly, $\frac{\partial w}{\partial x}$and $\frac{\partial w}{\partial y}$ represent the inclinations about *x* and *y*-axes.

$$\begin{aligned} &u = \sum_{i=1}^{4} N_i u_i, \quad v = \sum_{i=1}^{4} N_i v_i, \quad w = \sum_{i=1}^{4} N_i w_i, \\ &\theta_x = \sum_{i=1}^{4} N_i \theta_x^i, \quad \theta_y = \sum_{i=1}^{4} N_i \theta_y^i, \\ &\frac{\partial w}{\partial x} = \sum_{i=1}^{4} N_i \frac{\partial w_i}{\partial x}, \quad \frac{\partial w}{\partial y} = \sum_{i=1}^{4} N_i \frac{\partial w_i}{\partial y} \end{aligned} \tag{19}$$

where $\{q_{(e)}\}=\{u_i,\ v_i,\ w_i, \frac{\partial wi}{\partial x}, \frac{\partial wi}{\partial y}\}i=1,2,3,4$ nodal displacement vector.

N_i, *i=1, 2, 3, 4* denote the part nodal profile functions.

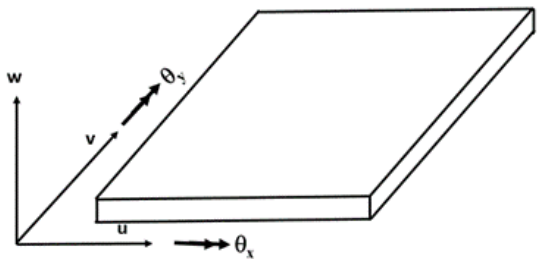

Fig.3. Rectangular element geometry

The part shape function matrix *[N]* can be written as follows:

$$[N]=\begin{Bmatrix}[N_{u_n}][N_{v_n}][N_{w_n}]\\ [N_{\theta_x}][N_{\theta_y}]\\ [N_{\partial w/\partial x}][N_{\partial w/\partial y}]\end{Bmatrix}^T \tag{20}$$

By applying higher-order shear deformation condition, the vibratory stresses of the plate element in strain energy can be expressed as below:

$$U_P^{(e)}=\frac{1}{2}\int_0^b\int_0^a\begin{bmatrix}[N]^T\{\varepsilon^{(n)}\}+[M]^T\{\varepsilon^{(1)}\}\\ +[P]^T\{\varepsilon^{(3)}\}\\ +[Q^s]^T\{\gamma^{(n)}\}+[R^s]^T\{\gamma^{(2)}\}\end{bmatrix}dxdy \tag{21}$$

The nodal displacement vector in the strain vector is expressed as below:

$$\{\varepsilon_{bd}^{(e)}\}=[B_{bd}]\{q_{(e)}\} \tag{22}$$

$$\{\gamma_{sh}^{(e)}\}=[B_{sh}]\{q_{(e)}\} \tag{23}$$

here, $[B_{(bd)}]=[B_{(b1)}]+z[B_{(b2)}]+z^3[B_{(b3)}]$ and $[B_{sh}]=[B_{s3}]+z^2[B_{s4}]$.

Replacing equations (13), (22) and (23) in equation (21), the potential energy of the plate part can be described as follows:

$$U_{PT}^{(e)}=\frac{1}{2}\{q_{(e)}\}^T\left([K_{(bd)}^{(e)}]+[K_{(sh)}^{(e)}]\right)\{q_{(e)}\} \tag{24}$$

The stiffness matrix of the element can be determined as below:

$$[K_{(e)}]=[K_{(bd)}^{(e)}]+[K_{(sh)}^{(e)}] \tag{25}$$

Hygrothermal stresses on the FGM plate when exposed to moisture and temperature. Those stresses are derived as follows:

$$\begin{Bmatrix}\sigma_{xx}^{hy}\\ \sigma_{yy}^{hy}\\ \tau_{xy}^{hy}\end{Bmatrix}=\begin{bmatrix}q_{11}&q_{12}&0\\ q_{21}&q_{22}&0\\ 0&0&q_{66}\end{bmatrix}\left[\begin{Bmatrix}1\\1\\0\end{Bmatrix}(\psi(z)\Delta T(z))+\begin{Bmatrix}1\\1\\0\end{Bmatrix}\varphi(T)\Delta C(z)\right] \tag{26}$$

where $q_{11}=q_{22}=\frac{E(z)}{(1-\nu^2(z))}$, $q_{12}=q_{21}=\frac{\nu(z)E(z)}{(1-\nu^2(z))}$ $q_{66}=\frac{E(z)}{2(1+\nu(z))}$, $\Delta C=C_c-C_m$, similarly $\Delta T=T_c-T_m$, anywhere T_m and C_m are the implication of heat and the represents moisture concentration at the metal surface, T_c and C_c are the temperature and moisture concentration at ceramic surface, respectively. Moreover, Ψ is the coefficient of thermal expansion of the plate; Φ is the moisture expansion coefficients of the FGM plate.

As a result of moisture concentration, the resultants of force, moments and moments of higher order are expressed as

$$\left.\begin{bmatrix}K_{xx}^{hy}\\ K_{yy}^{hy}\end{bmatrix}=\int_{-h/2-d}^{h/2-d}\begin{bmatrix}\sigma_{xx}^{hy}\\ \sigma_{yy}^{hy}\end{bmatrix}dz'\right.$$
$$\left.\begin{bmatrix}H_{xx}^{hy}\\ H_{yy}^{hy}\end{bmatrix}=\int_{-h/2-d}^{h/2-d}\begin{bmatrix}\sigma_{xx}^{hy}\\ \sigma_{yy}^{hy}\end{bmatrix}z'dz'\right. \tag{27}$$
$$\left.\begin{bmatrix}M_{xx}^{hy}\\ M_{yy}^{hy}\end{bmatrix}=\int_{-h/2-d}^{h/2-d}\begin{bmatrix}\sigma_{xx}^{hy}\\ \sigma_{yy}^{hy}\end{bmatrix}z'^3dz'\right.$$

Substituting eq. (26) in eq. (27) yields the following relations as follows:

$$\begin{bmatrix}K^{hy}\\ H^{hy}\\ M^{hy}\end{bmatrix}=\begin{bmatrix}[A^{hy}]&[B^{hy}]&[E^{hy}]\\ [B^{hy}]&[D^{hy}]&[F^{hy}]\\ [E^{hy}]&[F^{hy}]&[H^{hy}]\end{bmatrix}\begin{Bmatrix}\varepsilon^{(n)hy}\\ \varepsilon^{(1)hy}\\ \varepsilon^{(3)hy}\end{Bmatrix}, \tag{28}$$

The hygrothermal stiffness elements are computed as below:

$$\begin{aligned}&\left(G_{lm}^{hy}\quad L_{lm}^{hy}\quad V_{lm}^{hy}\quad E_{lm}^{hy}\quad L_{lm}^{hy}\quad J_{lm}^{hy}\right)\\ &=\int_{-h/2}^{h/2}q_{lm}^{(k)}\left(\psi(z)\Delta T(z)+\varphi(z)\Delta C(z)\right)\left(1,z,z^2,z^3,z^4,z^6\right)dz\\ &(l,m=1,2)\end{aligned} \tag{29}$$

The relationships of strain-displacement with a respective neutral plane can be derived as follows:

$$\begin{aligned}\{\varepsilon^{(b)hy}\}&=\begin{Bmatrix}\varepsilon_x^{hy}\\ \varepsilon_y^{hy}\end{Bmatrix}\\ &=\begin{Bmatrix}\varepsilon_x^{(n)hy}\\ \varepsilon_y^{(n)hy}\end{Bmatrix}+z\begin{Bmatrix}\varepsilon_x^{(1)hy}\\ \varepsilon_y^{(1)hy}\end{Bmatrix}-z^3\begin{Bmatrix}\varepsilon_x^{(3)hy}\\ \varepsilon_y^{(3)hy}\end{Bmatrix}\end{aligned} \tag{30}$$

The expression for strain vector is formulated in expressions of a nodal vector of displacements $\{q_{(e)}\}$ can be described as:

$$\{\varepsilon_{hy}^{(bd)}\}=[B_{(bd)}]\{q_{(e)}\} \tag{31}$$

where $[B_b]=[B_b]+z'[B_1]+z'^3[B_2]$

The component strain energy $(U_{HT}^{(e)})$ of the element due to temperature rise and moisture concentration is expressed as below:

$$U_{HT}^{(e)}=\frac{1}{2}\int_0^b\int_0^a\begin{bmatrix}[K^{hy}]^T\{\varepsilon^{(n)hy}\}+\\ [H^{hy}]^T\{\varepsilon^{(1)hy}\}+\\ [M^{hy}]^T\{\varepsilon^{(3)hy}\}\end{bmatrix}dxdy \tag{32}$$

Replacing comparisons of Eq. (30) and Eq. (31) in Eq. (32), the element strain energy as a result of moisture concentration can be formulated as below:

$$U_{(hy)}^{(e)} = \frac{1}{2}\left\{q_{(e)}\right\}^T \left[K_{(hy)}^{(e)}\right]\left\{q_{(e)}\right\} \tag{33}$$

Expression of matrix $[K_{(hy)}^{(e)}]$ is given in element resultant strain energy $(U^{(e)})$.

$$\begin{aligned} U^{(e)} &= U_{(pe)}^{(e)} - U_{(hy)}^{(e)} \\ &= \frac{1}{2}\left[\left\{q_{(e)}\right\}^T \left[K^{(e)}\right]\left\{q_{(e)}\right\}\right] \\ &\quad -\frac{1}{2}\left[\left\{q_{(e)}\right\}^T \left[K_{(hy)}^{(e)}\right]\left\{q_{(e)}\right\}\right] \\ &= \frac{1}{2}\left\{q_{(e)}\right\}^T \left[K_{(fn)}^{(e)}\right]\left\{q_{(e)}\right\} \end{aligned} \tag{34}$$

where $[K_{(fn)}^{(e)}] = [K^{(e)}] - [K_{(hy)}^{(e)}]$

The plate element kinetic energy is derived as follows:

$$T^{(e)} = \frac{1}{2}\int_v \rho(z')\left(\dot{u}^2 + \dot{v}^2 + \dot{w}^2\right)dv \tag{35}$$

The shape functions and nodal velocity vectors $\dot{u}, \dot{v}$ and $\dot{w}$ are represented as below:

$$\begin{aligned} \dot{u} &= \left[\left[N_{u_n}\right] + z'\left[N_{\theta_x}\right] - c_1 z'^3\left(\left[N_{\theta_x}\right] + \left[N_{\partial w/\partial x}\right]\right)\right]\left\{\dot{q}^{(e)}\right\}^T, \\ \dot{v} &= \left[\left[N_{v_n}\right] + z'\left[N_{\theta_y}\right] - c_1 z'^3\left(\left[N_{\theta_y}\right] + \left[N_{\partial w/\partial y}\right]\right)\right]\left\{\dot{q}^{(e)}\right\}^T \end{aligned} \tag{36}$$

$$\dot{w} = \left[N_{w_n}\right]\left\{\dot{q}^{(e)}\right\}^T$$

$$T^{(el)} = \frac{1}{2}\left[\left\{\dot{q}_{(e)}\right\}^T \left[M_{(el)}\right]\left\{\dot{q}_{(e)}\right\}\right] \tag{37}$$

anywhere $[M_{(e)}]$ is the matrix of element mass.

The elemental work done can be written in terms of nodal displacement vector as follows:

$$\begin{aligned} WD_{(el)} &= \frac{1}{2}\int_A \left\{q_{(e)}\right\}^T \begin{bmatrix} P(t)\left[\partial w/\partial x\right]^T\left[\partial w/\partial x\right] + \\ P(t)\left[\partial w/\partial y\right]^T\left[\partial w/\partial y\right] \end{bmatrix}\left\{q_{(e)}\right\} dx\,dy \\ &= \frac{1}{2}\left\{q_{(e)}\right\}^T \left(P(t)\right)\left[K_{(el)}^{(G)}\right]\left\{q_{(e)}\right\} \end{aligned} \tag{38}$$

here $[K_{(el)}^{(G)}]$ is the matrix of the stiffness related to geometry.

$$\left[K_{(el)}^{(G)}\right] = \int_0^l\int_0^w \begin{bmatrix} \left[\partial w/\partial x\right]^T\left[\partial w/\partial x\right] + \\ \left[\partial w/\partial y\right]^T\left[\partial w/\partial y\right] \end{bmatrix} dx\,dy \tag{39}$$

3. Directing Equation of Motion

In the hygrothermal environment, the governing equation of movement about FGM plate has been established applying Hamilton's principle.

$$\delta\int_{t_1}^{t_2}\left(T^{(e)} - U^{(e)} + W^{(e)}\right)dt = 0 \tag{40}$$

In-plane loading on FGM plate, an arbitrary equation development of plate element represented as below:

$$\left[M^e\right]\left\{\ddot{q}^e\right\} + \left[K_{ef}^e\right]\left\{q^e\right\} - W(t)\left[K_g^e\right]\left\{q^e\right\} = 0 \tag{41}$$

The global matrices and displacement vector are obtained by assembling the element matrices, then the governing equation of motion of the plate element attained is expressed as:

$$[M]\{\ddot{q}\} + \left[K_{ef}\right]\{q\} - W(t)\left[K_g\right]\{q\} = 0 \tag{42}$$

Here $W(t) = \alpha P^{cr} + \beta P^{cr}\cos\Omega t$, the static load factor is α and the dynamic load factor is β, correspondingly.

$$[M]\{\ddot{q}\} + \left(\left[K_{ef}\right] - \alpha P^{cr}\left[K_g\right]\right)\{q\} - \beta P^{cr}\cos\Omega t\left[K_g\right]\{q\} = 0 \tag{43}$$

3.1. Analysis of dynamic stability

The solution of the governing equation of motion is acquired by Floquet's theory with periodic function. Fourier series with period $2T$ is deliberating for the periodic solution, and it can be expressed as below:

$$q(t) = \sum_{b=1,3,..}^{\infty}\left[\{c_b\}\sin\frac{b\Omega t}{2} + \{d_b\}\cos\frac{b\Omega t}{2}\right] \tag{44}$$

Contemplating first-order term (b=1) and it can be substituted in the Fourier series expansion of Eq. (44) in eq. (43). The coefficients of $cos\frac{\Omega t}{2}$ and $sin\frac{\Omega t}{2}$ terms comparison, solutions with period $2T$ is:

$$\left|\left[K_{ef}\right] - \left(\alpha \pm \frac{\beta}{2}\right)P^{cr} \times \left[K_g\right] - \frac{\Omega^2}{4}[M]\right| = 0 \tag{45}$$

The dynamic stability region would be obtained by plus and minus sign. The solution of the equation can be computed by the instability boundaries.

4. Results and Discussion

4.1. Validation of present work

For this study temperature, dependent materials are deliberated in order to analyze an all side's fixed FGM ($Si_3N_4/SUS304$) plate with a constant temperature field. Table 1 presents the material coefficients of temperature-dependent properties.

Frequency parameter: $\varpi = \frac{\omega W^2}{\Pi^2}\sqrt{\frac{I_0}{D}}$,

Here $I_0 = \rho h$, $D = \frac{E_m h^3}{12(1-\nu^2)}$ and base material as metal SUS304 at room temperature $T = 300$ K is assumed.

The expansion coefficient of moisture constants for ceramic $\Phi_c = 0$ and for metal $\Phi_m = 0$ are adopted from literature [22].

A 10×10-element discretization gives satisfactory convergence for the natural frequencies of the plate. The contemporary computational purpose acquired outcomes are correlated by published outcomes. For comparative study, the first six mode natural frequencies of all sides' fixed FGM plates are contemplated. The present method results are accomplished by applying a third-order shear deformation hypothesis. Senthil, Batra [6], Yang, and Shen [7] results matched the present mathematical results.

Table 2 results reveal the primary six fundamental frequency parameters of a plate made of (Si3N4/SUS304) FGM, here, the ceramic rich of an upper surface and metal-rich of the bottom surface. The uniform temperature rise environment is chosen for this study with index values k = 2 and 10 and geometric properties L/W = 1.0 and 1.5. Senthil [6] and Yang [7] results are compared with the present computational method and found to be in good agreement.

The influence of moisture percentage on the fundamental natural frequency of the laminated composite (Graphite/Epoxy) plate is listed in Table 3. The results are in agreement with the earlier work of reference [16].

4.2. FGM plates free vibration and buckling study

An FGM (Al2O3/SUS305) plate with geometrical properties of thickness 0.02m and 0.2m of length has been deliberating for this analysis. The computational results of natural frequencies are obtained with various thermal fields. All sides simply supported FGM plate by nonlinear, linear and uniform thermal fields are contemplating and the analyzed results are presented graphically. The thermal environment of nonlinear, linear and uniform fields are presented in Figs. 4 (a), 5 (a) and 6 (a) for the deviation of primary regularity parameter with index value k=1 and 5, correspondingly. Moreover, the depicted Figs. 4 (b), 5 (b), and 6 (b) display the distinction of frequency parameters in the secondary mode of simply defended FGM plate by linear, constant and nonlinear heat circumstances with k=1 and 5 index values, respectively.

Table 1. Material properties of temperature-dependent Reddy and Chin [4]

Materials	Units	P_0	P_{-1}	P_1	P_2	P_3
Al_2O_3	E (Pa)	$349.55X10^9$	0	$-3.853x10^{-4}$	$4.027x10^{-7}$	-1.67310^{-11}
	ψ (/K)	$6.8269x10^{-6}$	0	$1.838x10^{-4}$	0	0
	v	0.26	0	0	0	0
	ρ(kg/m³)	2700	0	0	0	0
Si_3N_4	E (Pa)	$348.43X10^9$	0	$-3.070x10^{-4}$	$2.160x10^{-7}$	-8.94610^{-11}
	ψ (/K)	$5.872x10^{-6}$	0	$9.065x10^{-4}$	0	0
	v	0.24	0	0	0	0
	ρ(kg/m³)	2370	0	0	0	0
SUS304	E (Pa)	$201.04x10^9$	0	$3.079x10^{-4}$	$-6.534x10^{-7}$	0
	ψ (/K)	$2.33x10^{-6}$	0	$8.086x10^{-4}$	0	0
	v	0.3262	0	$-2.002x10^{-4}$	$3.797x10^{-7}$	0
	ρ(kg/m³)	8166	0	0	0	0

Table 2. comparison of all side clamped (Si_3N_4/SUS304) FGM plates of first six frequency parameters

			Frequency parameters					
L/W	k	Source	ω_1	ω_2	ω_3	ω_4	ω_5	ω_6
1	2	Yang [7]	3.663	7.254	7.254	10.392	11.705	12.317
		Senthil [6]	3.720	7.301	7.301	10.334	12.225	12.356
		Present	3.661	7.283	7.283	10.254	12.520	12.655
	10	Yang [7]	3.183	6.300	6.300	9.017	10.237	10.678
		Senthil [6]	3.139	6.185	6.185	8.765	10.372	10.486
		Present	3.103	6.278	6.278	8.821	10.565	10.682
1.5	2	Yang [7]	2.733	4.223	6.633	6.633	7.908	9.812
		Senthil [6]	2.790	4.283	6.640	6.722	7.894	9.852
		Present	2.757	4.221	6.663	6.677	7.847	9.876
	10	Yang [7]	2.3753	3.667	5.761	5.761	6.869	8.520
		Senthil [6]	2.3470	3.614	5.623	5.691	6.688	8.355
		Present	2.3058	3.540	5.611	5.619	6.611	8.326

Table 3. Comparison of moisture effect on the natural frequency parameter of the laminated plate.

Moisture percentage	0%	0.5%	1%	1.5%
Ref [16]	12.816	11.258	10.762	9.248
Present	12.726	11.171	10.649	9.164

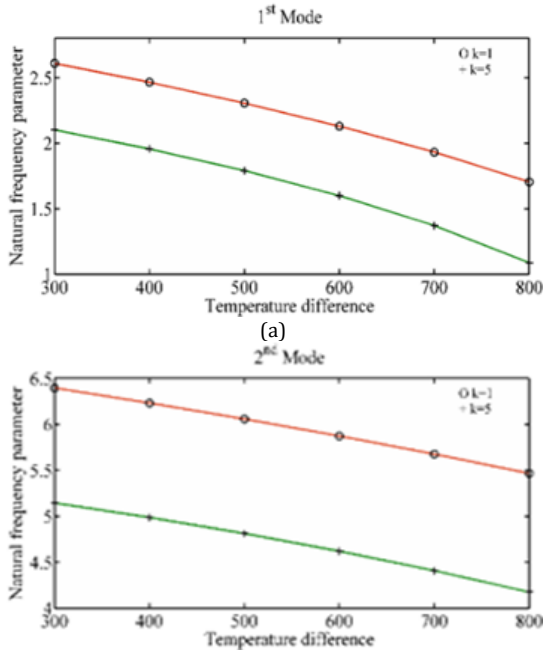

Fig.4. FGM plate natural frequency parameter variation in the uniform temperature field. (a) First Mode and (b) Seconde Mode.

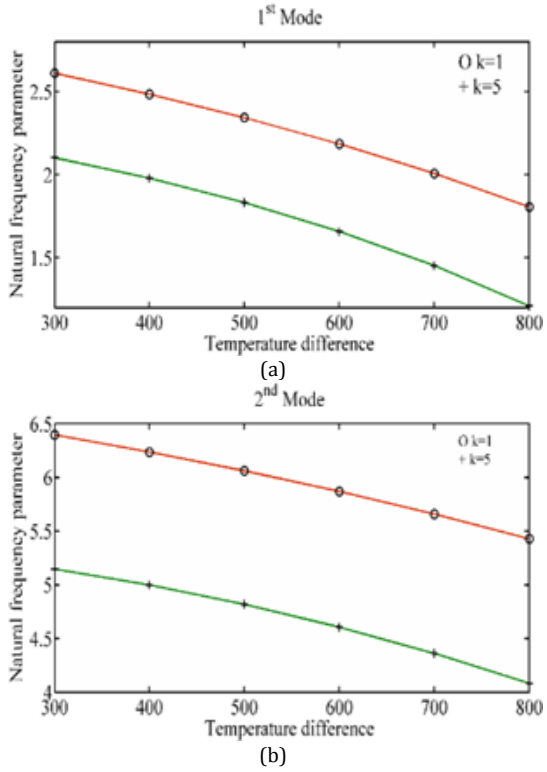

Fig. 5. FGM plate natural frequency parameter in the linear temperature field. (a) First Mode and (b) Seconde Mode.

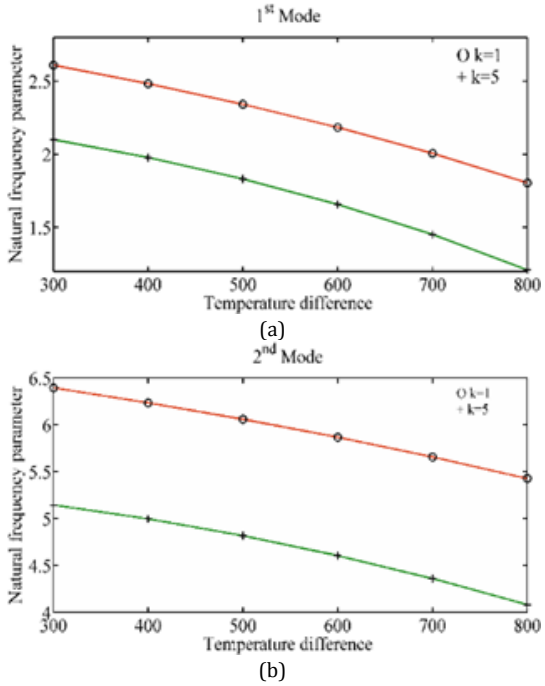

Fig. 6. (a) FGM plate natural frequency parameter in the nonlinear temperature field. (a) First Mode and (b) Seconde Mode.

These influence the various thermal environments on the natural frequencyy of the first mode as depicted in Fig. 7. It describes that the uniform thermal field is more intense compared with the linear and nonlinear thermal fields. As a result of this, the uniform temperature field affects more significantly on a natural frequency parameter than those of the nonlinear and linear thermal fields.

Figure 8 (a, b) reveals the influence of the moisture rate on the primary and secondary mode natural frequencies of the plate and the operating temperature, including the symbol consequences of k=1 and k=5, respectively. It is evident that the rise of moisture percentage decreases the primary and secondary mode frequency parameter of plates. The effective stiffness of the FGM plate is reduced through the rising of moisture fraction; consequently, the frequency parameters are decreased.

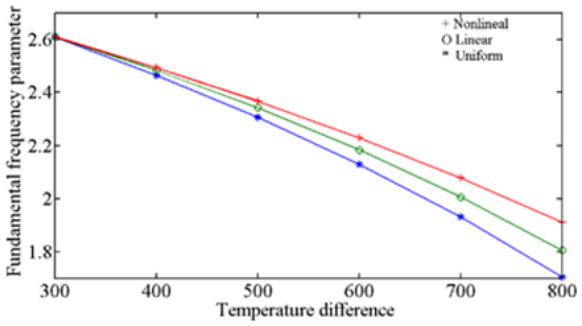

Fig. 7. First mode fundamental frequency parameter variation with temperature change for various heat filed. (K=1, ΔC=1%).

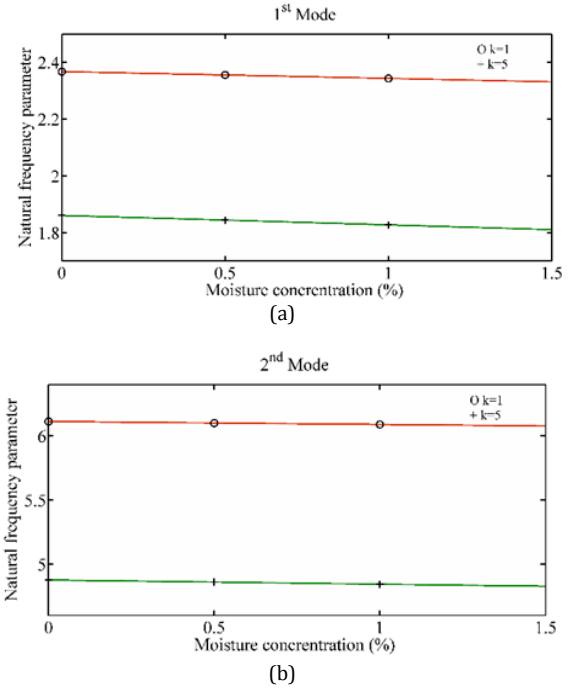

Fig. 8 Ppercentage variation of moisture versus frequency parameter of a plate. (a) First and (b) Secondary

The first and secondary mode fundamental frequency parameter variation regarding simply supported plates at $\Delta T = 500$ K is depicted in Fig. 9(a) and (b) with index values k = 2 and 10, correspondingly. The moisture concentration percentage varies from 0% to 1.5%. These Figures display that gaining moisture percentage declines the fundamental parameters. The presence of moisture concentration causes a significant reduction of non- dimensional parameters of the first two-mode frequencies, as it is observed in the plots.

The stiffness of the FGM plate in the hygrothermal field is reduced; as a result of the increase of moisture percentage, so the decreased stiffness reduces the natural frequencies. The effective elasticity of the modulus is reduced with an increase of metal volume fraction, so the frequency parameters decrease. Similarly, an increase of index value decreased the current elasticity of modulus and caused the reduction of natural frequency parameters.

The influence of variation regarding the percentage of moisture at the critical buckling of plates formed FGM under the hygrothermal field by symbol preferences k=1 also 5 as presented in Figs. 10 (a) and (b), respectively. The increase of moisture percentage from 0% to 1.5% causes a reduction of critical buckling load. The Figures portrayed the amount of moisture percentage, an increase that may cause loss of its structural properties and reduces critical buckling load.

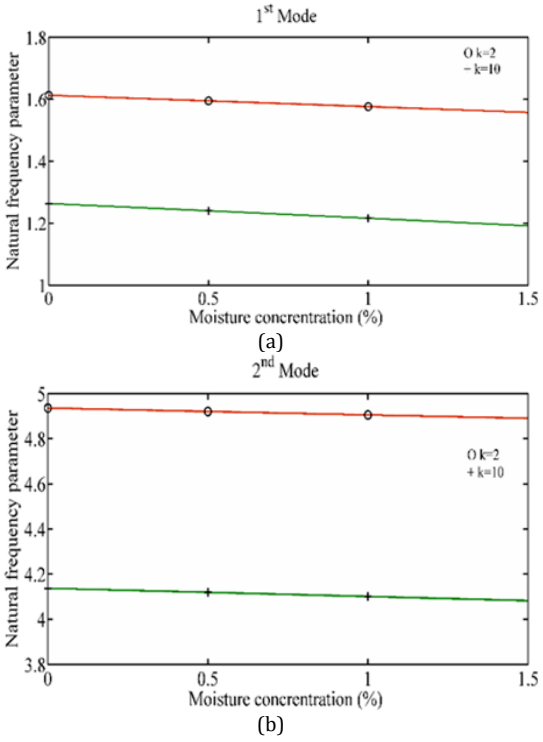

Fig. 9. Moisture concentration variation of natural frequency parameter. (a) First and (b) Second Mode.

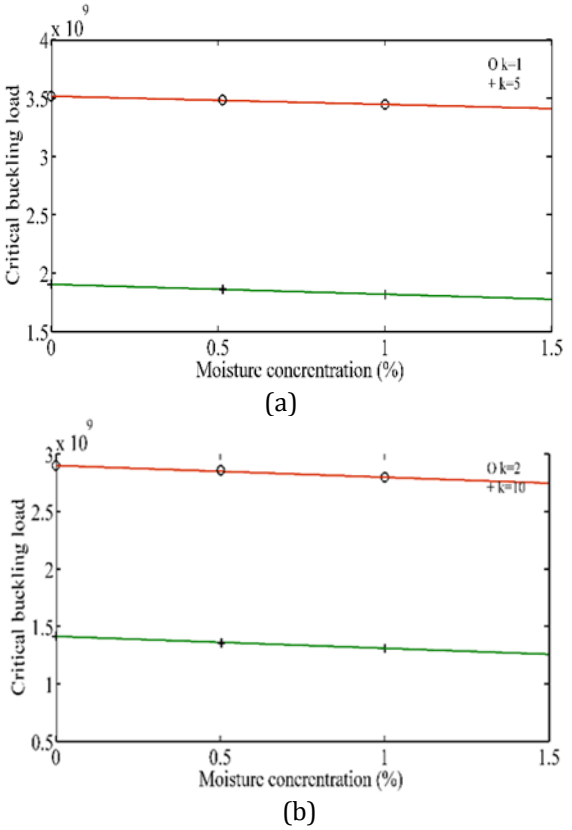

Fig. 10. Moisture concentration versus a critical bulking load of FGM plate (a) k=1 and 5, (b) k=2 and 10.

4.3. Influence of hygrothermal field on parametric instability of FGM plates

Figures 11 and 12 would highlight the dynamic stability regions of the FGM plates rise of

temperature at k=1 and k=5, correspondingly. The increase of temperature $0K$, $200K$ and $400K$ display the way the instability in the region changes towards the axis of the dynamic load. It indicates that the rise of temperature reduces the stability of the plate. The parametric resonance of excitation frequency is reduced with an increase in temperature. The structural stiffness is reduced with an increase in temperature, which causes more chances of loss of stability.

The influence of moisture on the parametric instability of the plate formed by FGM under the hygrothermal condition is illustrated in Figs. 13 and 14 with a constant temperature field (100 K).

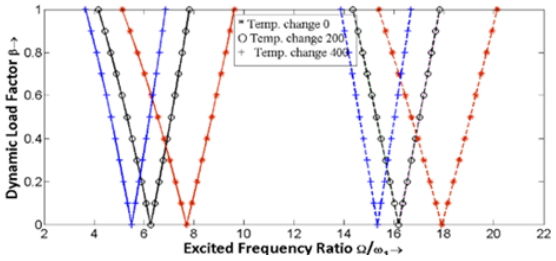

Fig. 11. The rise of temperature influences the parametric instability of the FGM plate at k=1.

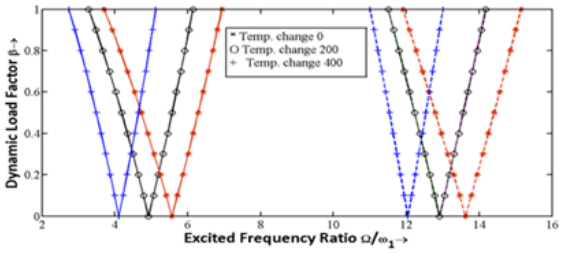

Fig. 12. The rise of temperature influences the parametric instability of the FGM plate at *k=5.*

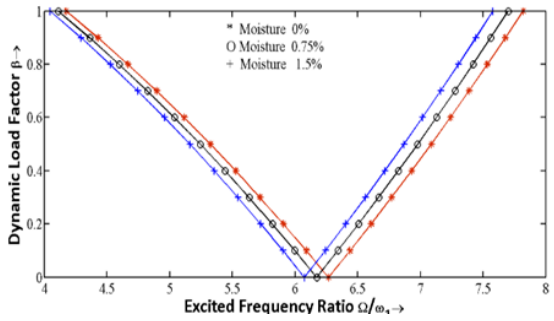

(a)

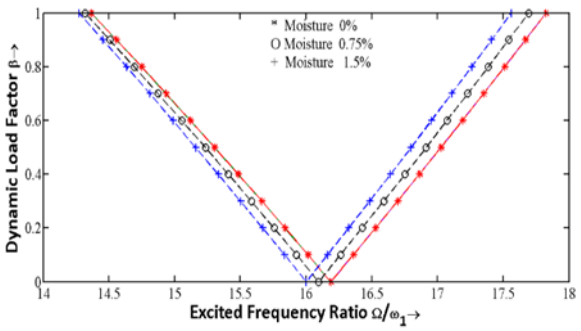

(b)

Fig. 13 Moisture concentration influence the uncertainty region of the plate (FG) at k=1. (a) first mode and (b) seconde mode

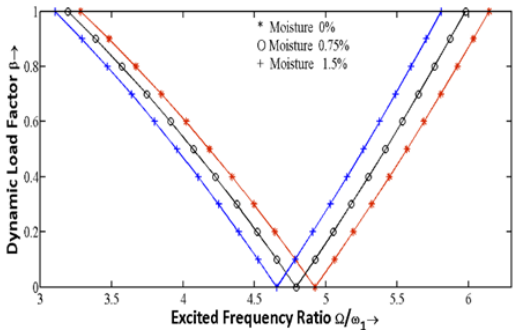

(a)

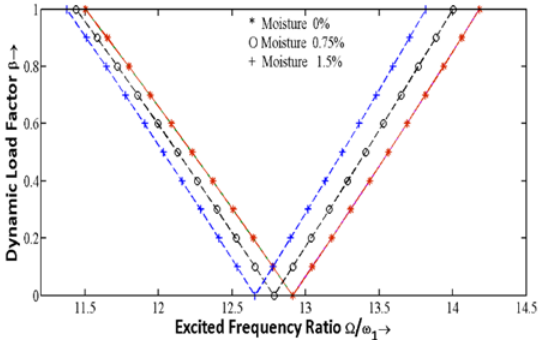

(b)

Fig. 14 Moisture concentration influence the secondary mode uncertainty area of the plate (FG) at k=5. (a) first mode and (b) second mode.

The moisture percentage concentration is depicted to be at 0%, 0.75% and 1.5%, so the increase of percentage concentration reduces the dynamic stability at value k=1 and k=5 of FGM plate. The parametric instability areas move near the axis of the dynamic load with the rise of moisture percentage. The excitation frequency lowers as a result to the boost in moisture concentration.

The various combinations of the temperature difference and percentage of moisture (100, 0.5%), (300, 1%) and (500, 1.5%) of hygrothermal environment conditions are investigated and depicted in Figs. 15 (a) and (b), respectively.

The dynamic instability graphs illustrated in Figs. 15 (a) and (b) reveal various combinations of moisture percentage and difference of temperature. It absorbs moisture from the plots and the temperature rise degrades the overall stiffness of the structure. The tainted FGM structure reduces the excitation frequency; it causes the instability area to move toward the axis of dynamic load. Hence, instability is enhanced for the FGM plate in the hygrothermal field. In addition to that, the area of instability increases and reveals the excitation frequencies range are wider.

Figures 16 (a) and (b) depict the influence of moisture percentage and rise of temperature on the parametric uncertainty of the plate by power-law unit k=5. The lesser excitation frequencies occur as a result of an increase of index value.

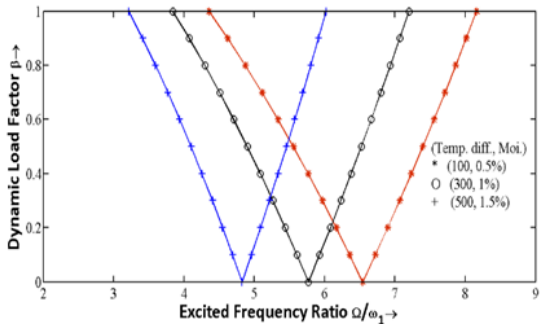

(a)

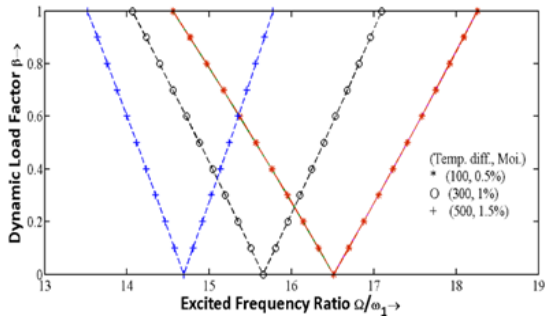

(b)

Fig. 15 Parametric uncertainty region of FG material plate in the hygrothermal field by k=1. (a) Fundamental and (b) Secondary

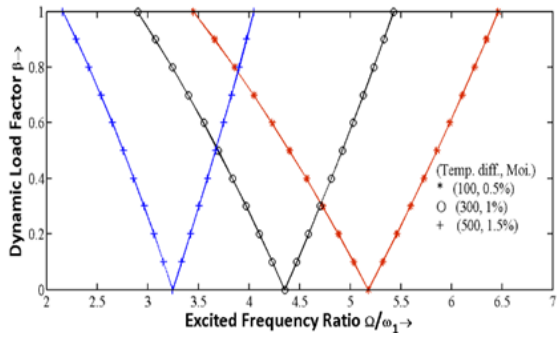

(a)

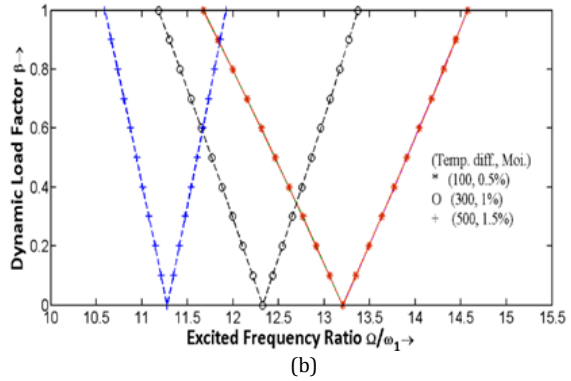

(b)

Fig.16 Uncertainty zone of FG material plate in the hygrothermal field with k=5. (a) First mode and (b) Second mode.

5. Conclusions

In this work, a finite element method applying a third-order shear deformation hypothesis in conjunction with Hamilton's principle for vibration and parametric instability of the FGM plates has been presented. The influence of the hygrothermal environment and index values on parametric instability of the FGM plate for simply supported boundary conditions was studied.

The variation of frequency parameter in uniform, linear and nonlinear thermal fields was computed; the boost of temperature difference decreases the primary and secondary mode fundamental frequencies of the FGM plate in each case respectively. Similarly, the fundamental frequencies of the initial and secondary modes are reduced by a rise concerning rule values. The heat enhancement and precipitation presence reduce the frequency parameters of FGM plates. The critical bulking load of the FGM plate is reduced with the rising of the moisture concentration.

The hygrothermal field increases temperature and the parametric instability of the FGM plate under periodic loading. The presence of moisture concentration stable the FGM plate makes less in a hygrothermal field. The parametric instability enhanced by the accumulation of moisture preoccupation. The lower excitation frequencies occur due to the mutual consequence of moisture concentration and the rise of heat in the parametric uncertainty region. It indicates that dynamic stability reduces the hygrothermal environment.

References

[1] Bolotin V V. **The dynamic stability of elastic systems**. Volume I. Aerospace Corporation, EI Segundo, California, 1962.

[2] Levinson M. An accurate, simple theory of the statics and dynamics of elastic plates. *Mechanics Research Communications* 1980; 7(6): 343-350.

[3] Zhang D, Zhou Y. A theoretical analysis of FGM thin plates based on physical neutral surface. *Computational Materials Science* 2008; 44: 716–720.

[4] Reddy JN, Chin CD. Thermomechanical analysis of functionally graded cylinders and plates. *J Thermal Stresses* 1998; 21: 593–629.

[5] Naghdabadi R, Hosseini SA. A finite element formulation for analysis of functionally graded plates and shells. *Archive of Applied Mechanics* 2005; 74: 375-386.

[6] Senthil Vel S, Batra RC. Three-dimensional exact solution for the vibration of functionally graded rectangular plates. *Journal of Sound and Vibration* 2004: 272: 703–730.

[7] Yang J, Shen HS. Vibration characteristics and transient response of shear-deformable functionally graded plates in thermal environments. *Journal of Sound and vibration* 2002; 255(3): 579-602.

[8] Kim Y W. Temperature dependent vibration analysis of functionally graded rectangular plates. *Journal of Sound and Vibration* 2005; 284: 531–549.

[9] Abrate S. Free vibration, buckling, and static deflections of functionally graded plates. *Composites Science and Technology* 2006; 66: 2383–2394.
[10] Croce LD, Venini P. Finite elements for functionally graded Reissner–Mindlin plates. *Computer Methods in Applied Mechanics and Engineering* 2004; 193: 705–725.
[11] Ramu I, Mohanty SC. Buckling Analysis of Rectangular Functionally Graded Material Plates under Uniaxial and Biaxial Compression Load. International Conference on Structural Integrity, In: Elsevier Procedia Engineering 86; 748–757: 2014.
[12] Ramu I, Mohanty SC. Modal analysis of Functionally Graded material Plates using Finite Element Method. 3rd International Conference Material Processing and Characterization. In: Procedia Materials Science 6; 460-467; 2014.
[13] Efraim E, Eisenberger M. Exact vibration analysis of variable thickness thick annular isotropic and FGM plates. *Journal of Sound and Vibration* 2007; 299: 720-738.
[14] Shahrjerdi F, Mustapha M, Bayat, D LA, Majid. Free vibration analysis of solar functionally graded plates with temperature-dependent material properties using second order shear deformation theory. *Journal of Mechanical Science and Technology* 2011; 25(9): 2195-2209.
[15] Lee Y, Kim JH. Hygrothermal effects on the structural behaviors of functionally graded plates. In: 19th annual international conference on composites/nano engineering (ICCE-19); 2011.
[16] Lee Y, Kim JH. Hygrothermal postbuckling behavior of functionally graded plates. *Composite Structures* 2013; 95: 278–282.
[17] Lal KR, Jagtap, Singh BN. Post buckling response of functionally graded materials plate subjected to mechanical and thermal loadings with random material properties. *Applied Mathematical Modelling* 2013; 37: 2900–2920.
[18] Ramu I, Mohanty SC. Flap wise bending vibration and dynamic stability of rotating functionally graded material plates in thermal environments. *Proceedings of the Institution of Mechanical Engineers, Part G: Journal of Aerospace Engineering* 2017; 231(2): 203-217.
[19] Wanga S, Dawe DJ. Dynamic instability of composite laminated rectangular plates and prismatic plate structures. *Computer Methods Applied Mechanics and Engineering* 2002; 191: 1791–1826.
[20] Rao VVS, Sinha PK. Dynamic response of multidirectional composites in hygrothermal environments. *Composite Structures* 2004; 64: 329–338.
[21] Rath MK, Dash MK. Parametric Instability of Woven Fiber Laminated Composite Plates in Adverse Hygrothermal Environment. *American Journal of Mechanical Engineering* 2014; 2(3): 70-81.
[22] Ramu I. On the dynamic stability of functionally graded material plates under parametric excitation. PhD thesis, National Institute of Technology, Rourkela, India, 2015.
[23] Ramu I, Narendra M, Venu M. Effect of hygrothermal environment on free vibration characteristics of FGM plates by finite element approach. International Conference on Mechanical, Materials and Renewable Energy. IOP Conference Series: Materials Science and Engineering, 377(1); 2018.
[24] Mohammad RezaBarati and HosseinShahverdi. Aero-hygro-thermal stability analysis of higher-order refined supersonic FGM panels with even and uneven porosity distributions. *Journal of Fluids and Structures* 2017; 73: 125-136.
[25] Mohammad Reza Baratim. Nonlocal stress-strain gradient vibration analysis of heterogeneous double-layered plates under hygro-thermal and linearly varying in-plane loads. *Journal of Vibration and Control* 2018; 24(19): 4630-4647.
[26] Bousahla, Abdelmoumen Anis, Benyoucef, Samir, Tounsi, Abdelouahed, Mahmoud SR. On thermal stability of plates with functionally graded coefficient of thermal expansion. *Structural Engineering and Mechanics* 2016; 60(2): 313–335.
[27] Bellifa H, Bakora A, Tounsi A, Bousahla A, Mahmoud SR. An efficient and simple four variable refined plate theory for buckling analysis of functionally graded plates. *Steel and Composite Structures* 2017; 25(3): 257–270.
[28] Mohammad Reza Barati, Hossein Shahverdi. Hygro-thermal vibration analysis of graded double-refined-nanoplate systems using hybrid nonlocal stress-strain gradient theory. *Composite Structures* 2017; 176: 982-995.
[29] Youcef Beldjelili, Abdelouahed Tounsi, Samy Hassan. Hygro-thermo-mechanical bending of S-FGM plates resting on variable elastic foundations using a four-variable trigonometric plate theory. *Smart Structures and Systems* 2016; 18(4): 755-786.
[30] Mohamed Zidi, Abdelouahed Tounsi, Mohammed Sid Ahmed Houari, Abbas Adda Bedia El, Anwar Bég O. Bending analysis of FGM plates under hygro-thermo-mechanical loading using a four variable refined plate

theory. *Aerospace Science and Technology* 2014; 34: 24-34.

[31] Farzad Ebrahimi and Mohammad Reza Barati. Small-scale effects on hygro-thermo-mechanical vibration of temperature-dependent nonhomogeneous nanoscale beams. *Journal Mechanics of Advanced Materials and Structures* 2017; 24(11): 924-936.

[32] Mohammad Reza Barati. Nonlocal microstructure-dependent dynamic stability of refined porous FG nanoplates in hygro-thermal environments. *The European Physical Journal Plus* 2017; 132(10): 434-442.

[33] Barati Mohammad Reza, Shahverdi, Hossein. Aero-hygro-thermal stability analysis of higher-order refined supersonic FGM panels with even and uneven porosity distributions. *Journal of Fluids and Structures* 2017; 73: 125-136.

[34] Abderrahmane Mouffoki, Adda Bedia EA, Houari MSA, Abdelouahed Tounsi, Samy Hassan. Vibration analysis of nonlocal advanced nanobeams in hygro-thermal environment using a new two-unknown trigonometric shear deformation beam theory. *Smart Structures Systems* 2017; 20(3): 369-383.

[35] Abdelmoumen Anis Bousahla, Samir Benyoucef, Abdelouahed Tounsi, Samy Hassan. On thermal stability of plates with functionally graded coefficient of thermal expansion. *Structural Engineering & Mechanics* 2016; 60(2):313-335.